Fast-forwarding quantum simulation with real-time quantum Krylov subspace algorithms

Cristian L. Cortes,[1,*] A. Eugene DePrince, III,[2,†] and Stephen K. Gray[1,‡]
[1]*Center for Nanoscale Materials, Argonne National Laboratory, Lemont, Illinois 60439, USA*
[2]*Department of Chemistry and Biochemistry, Florida State University, Tallahassee, Florida 32306-4390, USA*

(Received 11 July 2022; accepted 13 September 2022; published 6 October 2022)

Quantum subspace diagonalization (QSD) algorithms have emerged as a competitive family of algorithms that avoid many of the optimization pitfalls associated with parameterized quantum circuit algorithms. While the vast majority of QSD algorithms have focused on solving the eigenpair problem for ground-state, excited-state, and thermal observable estimations, there has been a lot less work in considering QSD algorithms for the problem of quantum dynamical simulation. In this work, we propose several quantum Krylov fast-forwarding algorithms capable of predicting long-time dynamics well beyond the coherence time of current quantum hardware. Our algorithms use real-time evolved Krylov basis states prepared on a quantum computer and a multireference subspace method to ensure convergence towards high-fidelity, long-time dynamics. In particular, we show that the proposed multireference methodology provides a systematic way of trading off circuit depth with classical postprocessing complexity. We also demonstrate the efficacy of our approach through numerical implementations for several quantum chemistry problems, including the calculation of the autocorrelation and dipole moment correlation functions.

DOI: 10.1103/PhysRevA.106.042409

I. INTRODUCTION

Quantum simulation remains one of the most promising applications of quantum computation due its potential impact on high-energy physics, cosmology, condensed-matter physics, atomic physics, and quantum chemistry. While the vast majority of quantum-simulation-based algorithms have been designed for the fault-tolerant quantum computing era [1–6], the current generation of noisy intermediate-scale quantum (NISQ) [7] computers limits the types of algorithms that could be implemented in the near term [8–11]. Variational quantum algorithms (VQAs) with parameterized quantum circuits have emerged as one of the leading methodologies capable of dealing with these constraints, and within this context, several NISQ-friendly quantum simulation algorithms have been proposed. These include the subspace variational quantum simulator [12], iterative approaches [13–15], and fast-forwarding approaches such as variational fast-forwarding [16], variational Hamiltonian diagonalization [17], and fixed-state variational fast-forwarding [18]. The overarching idea in all of these methods consists of using a variational wave function, $|\psi(\boldsymbol{\theta})\rangle = U(\boldsymbol{\theta})|\mathbf{0}\rangle$, defined with respect to a parameterized quantum circuit $U(\boldsymbol{\theta})$ and using a quantum-classical computer feedback loop to solve the optimization problem. In recent years, however, it has been shown that a wide variety of optimization problems relevant to VQAs can display nonconvexity and vanishing gradients, which can lead to fundamental optimization challenges [19–23]. In addition, these algorithms suffer from large measurement overheads which can lead to long run times [9,10].

In this regard, quantum subspace diagonalization (QSD) methods have emerged as an alternative approach to the conventional parameterized quantum circuit methodology [24–29]. QSD methods express the variational wave function as a linear combination of nonorthogonal quantum states that are independently prepared on a quantum computer. By design, this formulation solves a convex optimization problem that avoids the challenges associated with conventional VQAs and parameterized quantum circuits (i.e., NP-hardness and barren-plateau phenomena [20,22]). While the vast majority of QSD algorithms have been applied to ground-state [25,27,28,30], excited-state [26,31,32], and finite-temperature [33] observable estimations, there has been a lot less work in applying QSD algorithms to the problem of quantum dynamical simulation. We should note, however, that in classical-computer-based quantum dynamics simulations there is a long history of the use of QSD, including the pioneering work on the iterative Lanczos method by Park and Light [34].

To the best of our knowledge, the only work to consider the quantum dynamical simulation problem using QSD methods is that of Lim *et al.* [35], in which the authors proposed a quantum subspace diagonalization method where the nonorthogonal states are constructed from the set of cumulative K-moment states, $\mathbb{CS}_K = \mathbb{S}_0 \cup \mathbb{S}_1 \cup \mathbb{S}_2 \cdots \cup \mathbb{S}_K$, where $\mathbb{S}_p = \{U_{i_p} \cdots U_{i_2} U_{i_1} |\phi_o\rangle\}$. Here, it is assumed that the Hamiltonian can be written as a sum of unitaries U_i and $|\phi_o\rangle$ can be prepared efficiently on a quantum computer. If the set of unitaries U_i is tensor products of Pauli operators, the problem of finding the subspace matrices reduces to a measurement of the quantum state $|\phi_o\rangle$ in different Pauli bases and, by construction, avoids the use of a Hadamard test.

*Present address: QC Ware Corporation, Palo Alto, CA 94306; cris.cortes@qcware.com
†deprince@chem.fsu.edu
‡gray@anl.gov

In this paper, we build off the work by Lim *et al.* [35] and Stair *et al.* [27] and propose a multireference quantum Krylov fast-forwarding (QKFF) algorithm for quantum dynamical simulation. In particular, we show that the addition of multireference states provides a route towards high-fidelity, long-time quantum simulation with a small number of Trotter steps. Our approach provides a controlled trade-off between quantum complexity, defined with respect to circuit depth, and classical complexity, defined with respect to the postprocessing complexity (i.e., solving a large system of equations on a classical computer). Combined with the multifidelity estimation (MFE) protocol proposed in our previous work [31], our approach avoids the Hadamard test with the added benefit of using an ultracompact wave-function representation [30] that is not classically tractable. To demonstrate the potential of our approach, we present numerical experiments for various physical problems, including the calculation of the autocorrelation function and two-time dipole moment correlation function.

II. QUANTUM KRYLOV FAST-FORWARDING

Quantum dynamical simulation aims to solve the time-dependent Schrödinger equation ($\hbar = 1$ throughout),

$$i\,\partial_t\,|\psi(t)\rangle = \hat{H}\,|\psi(t)\rangle\,, \tag{1}$$

which describes the dynamics of a general many-body Hamiltonian $\hat{H}$ written as the sum of N-qubit Pauli terms, $\hat{H} = \sum_i^L h_i \hat{P}_i$, where h_i is a weighting coefficient and $\hat{P}_i$ is a general tensor product of N Pauli operators, $\hat{P}_i = \otimes_{k=1}^{N_i} \hat{\sigma}_{i_k}^{(m_k)}$, with m_k denoting the qubit number and i_k acting as a label for the type of Pauli operator $\{\hat{I}, \hat{\sigma}_x, \hat{\sigma}_y, \hat{\sigma}_z\}$. We assume that the Hamiltonian is time independent but do not impose any type of restrictions on the locality of the Hamiltonian, thereby making this approach applicable to a wide variety of physical problems of interest. The multireference quantum Krylov method proceeds by approximating the wave function $|\psi(t)\rangle$ by a linear combination of nonorthogonal quantum states,

$$|\psi(t)\rangle \approx |\psi_K(t)\rangle = \sum_{n=0}^{M-1}\sum_{r=1}^{R} c_{nr}(t)\,|\phi_{nr}\rangle\,, \tag{2}$$

where M corresponds to the single-reference Krylov subspace dimension and R corresponds to the total number of reference states. The choice of nonorthogonal states $|\phi_{nr}\rangle$ ultimately leads to a wide variety of hybrid quantum-classical algorithms with various algorithmic trade-offs [31]. In this work, we will consider the real-time evolved Krylov basis states which form an order-M Krylov subspace, $\mathcal{K}_M = \text{span}\{|r\rangle\,, e^{-i\hat{H}\tau}\,|r\rangle\,, e^{-i\hat{H}2\tau}\,|r\rangle\,, \ldots, e^{-i\hat{H}(M-1)\tau}\,|r\rangle\}$, where $|r\rangle$ corresponds to the rth reference state and the (n, r) nonorthogonal state is given by $|\phi_{nr}\rangle = e^{-i\hat{H}n\tau}\,|r\rangle$.

Substituting Eq. (2) into Eq. (1) and multiplying from the left by $\langle\phi_{n'r'}|$, we obtain the quantum subspace Schrödinger equation,

$$i\,\mathbf{S}\partial_t\mathbf{c}(t) = \mathbf{H}\mathbf{c}(t), \tag{3}$$

where $\mathbf{c}(t)$ is a $RM \times 1$ column vector of time-dependent expansion coefficients, while $\mathbf{H}$ and $\mathbf{S}$ are $RM \times RM$ subspace matrices defined as $[\mathbf{H}]_{n'r',nr} = \langle\phi_{n'r'}|\hat{H}|\phi_{nr}\rangle$ and $[\mathbf{S}]_{n'r',nr} = \langle\phi_{n'r'}|\phi_{nr}\rangle$, respectively. Fast-forwarding is achieved by solving the quantum subspace Schrödinger equation, Eq. (3), with respect to the expansion coefficients $\mathbf{c}(t)$. Numerically, the solution can be obtained in a variety of different ways, including the use of linear multistep methods and Runge-Kutta methods [36], which becomes relevant when the system size becomes large. However, to obtain a better theoretical understanding, we focus on the formal solution, written succinctly as

$$\mathbf{c}(t) = e^{-i\mathbf{S}^{-1}\mathbf{H}t}\mathbf{c}(0), \tag{4}$$

where the initial condition column vector $\mathbf{c}(0)$ is given by $\mathbf{c}(0) = \mathbf{S}^{-1}\mathbf{d}(0)$ and $\mathbf{d}(0) = (\langle\phi_{01}|\psi(0)\rangle\,, \langle\phi_{11}|\psi(0)\rangle\,, \ldots, \langle\phi_{(M-1)R}|\psi(0)\rangle)^T$. Note that $\mathbf{d}(0)$ corresponds to the first column of the overlap matrix $\mathbf{S}$ if the first reference state is equal to the initial state $|\psi(0)\rangle$. The evaluation of the matrix exponential in (4) provides an estimate of the complex-valued expansion coefficients $\mathbf{c}(t)$ for arbitrary times t, allowing for fast-forwarded predictions well beyond the coherence time of the quantum hardware. It is worth noting that the overlap matrix $\mathbf{S}$ can be poorly conditioned, as demonstrated in previous works [27,31], requiring special considerations when taking the matrix inverse. As suggested by Klymko *et al.* [30], we use singular-value decomposition [37,38] of $\mathbf{S}$, coupled with zeroing out singular values that fall below a threshold when the inverse is constructed (see also Appendix A).

While a single-reference-based QKFF algorithm could be used in practice, we found that such an approach is severely limited in predicting long-time dynamics with a small number of Trotter steps. As a result, our main contribution corresponds to the proposal of a *multireference, selected* quantum Krylov fast-forwarding (SQKFF) algorithm for predicting long-time quantum dynamics with high fidelity, as summarized in Fig. 1. The algorithm starts with a single reference state which is equal to the initial quantum state supplied by the user. The projected subspace matrix elements ($[\mathbf{H}]_{n'r',nr}$ and $[\mathbf{S}]_{n'r',nr}$) are then estimated on the quantum computer using either the Hadamard test or MFE protocol [31]. A classical computer is then used to find the solution to the quantum subspace Schrödinger equation. If a stopping criterion is met, the SQKFF algorithm terminates; otherwise, the algorithm continues by selecting additional reference states based on a selection process that we will discuss later. Once the new reference states are selected, the previous three steps are repeated until the stopping criterion is met.

a. Reference selection process. The reference selection process is critical for the SQKFF algorithm. While many choices exist, we propose a simple approach that requires negligible circuit depth when compared to the Trotterized circuits required for real-time Hamiltonian simulation. Here, the basic idea corresponds to performing transition-probability measurements based on the user-defined initial state $|\psi(0)\rangle$. The transition-probability measurement procedure consists of two substeps: (1) preparing the Mth Krylov subspace state, $|\phi_{M-1,1}\rangle = e^{-i\hat{H}(M-1)\tau}\,|\psi(0)\rangle$, on the quantum computer and (2) performing sampling measurements in the Pauli Z basis (see Fig. 1). The frequency of the measured bit strings will follow an underlying transition-probability distribution,

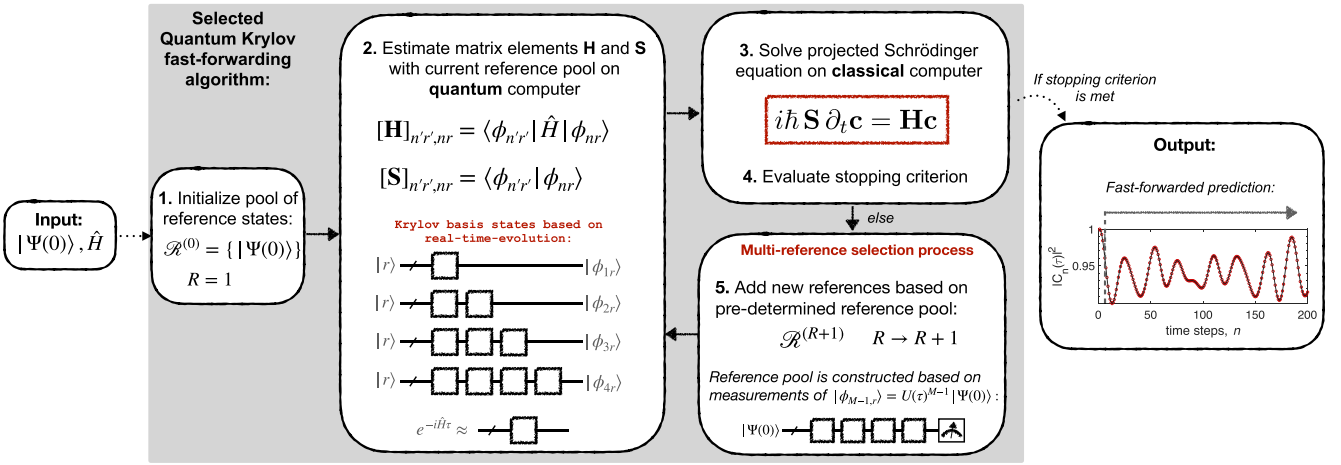

FIG. 1. Overview of the selected quantum Krylov fast-forwarding (SQKFF) method.

$p(x) = |\langle x|e^{-i\hat{H}(M-1)\tau}|\psi(0)\rangle|^2$. Assuming K total samples, the bit strings with the largest observed transition probabilities, n_x/K, are added to the reference pool $\mathcal{R}^{(R)}$, where n_x refers to the number of times the xth bit string was observed. While a complete determination of $p(x)$ scales exponentially with system size, we have found that relatively modest sampling suffices; typically, K on the order of hundreds or thousands of samples provided good estimates. Individual bit strings are added as reference states iteratively until our stopping criterion is met. To ensure that the superposition of bit strings preserves any symmetries inherent in the underlying Hamiltonian, a separate subspace Hamiltonian can be constructed with the sampled bit strings which is then diagonalized on the classical computer. The resulting eigenvectors will provide the numerical values for the amplitudes of the bit strings, ensuring that all of the Hamiltonian symmetries are preserved.

b. Stopping criterion. A pragmatic stopping condition is to specify some maximum time $T_{\max}$ of physical interest and an acceptable tolerance ϵ for some desired dynamical property such as the magnitude of a correlation function. If for times $t \leqslant T_{\max}$ the addition of more reference states yields changes no greater than ϵ in the dynamical property, then stop.

III. TIME-DEPENDENT OBSERVABLES

The solution to the projected subspace Schrödinger equation provides an estimate of the complex-valued coefficients $\mathbf{c}(t)$. Once these coefficients have been determined, it is then possible to calculate a wide variety of time-dependent observables through additional postprocessing that may or may not require additional calls to the quantum computer. In the following, we consider three different time-dependent quantities that are relevant to quantum chemistry, nuclear physics, and materials-science calculations: (1) the autocorrelation function, (2) time-dependent local and global observables, and (3) two-time correlation functions.

(1) The autocorrelation function, $C(t) = \langle\psi(0)|\psi(t)\rangle$, is perhaps the only time-dependent quantity that does not require any additional calls to the quantum computer based on the quantum Krylov method that we have outlined above. In general, we can write the approximate autocorrelation function as $C(t) = \sum_n c_n(t)\,\langle\psi(0)|\phi_n\rangle = \mathbf{d}^\dagger(0)\cdot\mathbf{c}(t)$, which is clearly expressed in terms of quantities that originate from the SQKFF algorithm.

(2) Time-dependent observables are often desirable for predicting physical quantities such as charge densities and order parameters. Based on the linear combination of nonorthogonal state expression from Eq. (2), a general time-dependent observable may be written as

$$O(t) = \langle\psi(t)|\hat{O}|\psi(t)\rangle = \sum_{k',k} c^*_{k'}(t)c_k(t)\,\langle\phi_{k'}|\hat{O}|\phi_k\rangle\,, \tag{5}$$

where we used the single index $k = nr$ to simplify the notation. Based on Eq. (5), it is clear that the fast-forwarded prediction for $O(t)$ might require additional calls to the quantum computer for evaluating the matrix elements, $[\mathbf{O}]_{n'r',nr} = \langle\phi_{n'r'}|\hat{O}|\phi_{nr}\rangle$. Assuming that the observable $\hat{O}$ is expressed as a linear combination of Pauli words, $\hat{O} = \sum_i^{L_o} o_i\hat{P}_i$, this implies that additional calls would be required for Pauli words that do not coincide with the Pauli words from the original Hamiltonian decomposition, $\hat{H} = \sum_i^L h_i\hat{P}_i$. In the worst case, this would require an additional $O(L_o(RM)^2)$ calls to the quantum computer, where L_o is equal to the total number of Pauli terms for observable, $\hat{O}$.

(3) Last, we consider the evaluation of two-time correlation functions of the form $\langle A(t+\tau)B(t)\rangle$, which are used for the calculation of two-particle correlation functions, Green's functions, and dipole moment correlation functions relevant to many different types of spectroscopies [39–44]. A general two-time correlation function between observables $\hat{A}$ and $\hat{B}$ may be written as

$$\langle A(t+\tau)B(t)\rangle = \langle\psi(t+\tau)|\hat{A}e^{-i\hat{H}\tau}\hat{B}|\psi(t)\rangle = \sum_{k',k} c^*_{k'}(t+\tau)c_k(t)\,\langle\phi_{k'}|\hat{A}e^{-i\hat{H}\tau}\hat{B}|\phi_k\rangle\,. \tag{6}$$

While $c_k(t)$ and $c^*_{k'}(t+\tau)$ are readily obtained from the original SQKFF algorithm evaluated with respect to the initial condition $|\psi(0)\rangle$, it is clear from Eq. (6) that the fast-forwarded prediction for the two-time correlation function $\langle A(t+\tau)B(t)\rangle$ requires the evaluation of $\langle\phi_{k'}|\hat{A}e^{-i\hat{H}\tau}\hat{B}|\phi_k\rangle$, which in turn requires a fast-forwarded

prediction of the time-evolved quantum state $|\tilde{\psi}(\tau)\rangle = e^{-i\hat{H}\tau}\hat{B}\,|\phi_k\rangle = \sum_{k''} c_{k''}(\tau)\,|\phi_{k''}\rangle$, leading to the evaluation of $\langle\phi_{k'}|\hat{A}e^{-i\hat{H}\tau}\hat{B}|\phi_k\rangle = \sum_{k''} c_{k''}(\tau)\,\langle\phi_{k'}|\hat{A}|\phi_{k''}\rangle$. This shows that an observable estimate of $\langle\phi_{k'}|\hat{A}|\phi_{k''}\rangle$ would also be required for the evaluation of the two-time correlation function when $\hat{A} \neq \hat{B}$. This implies that in the most general case, without additional simplifications, two separate runs of the SQKFF algorithm will be required for the prediction of two-time correlation functions. The first run will provide a fast-forwarded prediction for $|\psi(t)\rangle = e^{-i\hat{H}t}\,|\psi(0)\rangle$, while the second run will provide a fast-forwarded prediction of $|\tilde{\psi}(\tau)\rangle$. For many physical problems of interest, however, it will be possible to reduce this requirement.

To illustrate this point, we consider the calculation of the two-time dipole moment correlation function, $\langle\hat{\mu}_\xi(t+\tau)\hat{\mu}(t)\rangle = \langle\Psi_G|\hat{\mu}_\xi(t+\tau)\hat{\mu}_\xi(t)|\Psi_G\rangle$, where $|\Psi_G\rangle$ corresponds to the ground-state wave function of an electronic structure Hamiltonian $\hat{H}$ and the dipole moment operator, $\hat{\mu}_\xi = \sum_{pq}\mu^\xi_{pq}a^\dagger_p a_q$, is defined in the fermionic second quantized spin-orbital basis (additional details of the dipole moment correlation function and its evaluation are discussed in Appendix B). The dipole moment correlation function is a fundamental quantity of interest for chemistry and materials science because of its relation to the linear absorption spectrum. Details of this relationship can be found in Appendix C. To compute the two-time dipole moment correlation function, we first require preparing the ground-state wave function on the quantum computer. The preparation of the ground state can proceed in several ways and may certainly represent a challenge of its own. Here, we outline two methods that are amenable to near-term quantum computing. The first method assumes the use of a separate quantum Krylov diagonalization algorithm for ground-state energy estimation [26,27,30,31], which is able to express the ground-state wave function as a linear combination of nonorthogonal states, $|\psi_G\rangle \approx \sum_{n=0}^{M_G-1} c_n\,|\phi_n\rangle$, where the coefficients c_n are notably different from those in Eq. (2). Assuming that we have M_G nonorthogonal states in order to represent the ground-state wave function, the total run time of the SQKFF algorithm will increase by a multiplicative factor of M_G^2. The second methodology does not suffer from the increased run time and relies on using the results of a variational quantum eigensolver algorithm to find the approximate ground-state wave function, $|\psi_G\rangle \approx |\psi(\boldsymbol{\theta})\rangle = U(\boldsymbol{\theta})\,|0\rangle^{\otimes N}$, where $U(\boldsymbol{\theta})$ represents the parameterized quantum circuit unitary. Assuming that the approximate ground-state wave function from either method is written as $|\tilde{\Psi}_G\rangle$, it is then possible avoid the requirement of running two separate SQKFF algorithms by using the commonly used approximation $|\psi(t)\rangle = e^{-i\hat{H}t}\,|\tilde{\Psi}_G\rangle \approx e^{-i\tilde{E}_G t}\,|\tilde{\Psi}_G\rangle$, where $\tilde{E}_G$ is the ground-state energy that would have been estimated from either method. Once this approximation is invoked, the two-time dipole moment correlation function becomes $\langle\hat{\mu}_\xi(t+\tau)\hat{\mu}(t)\rangle = e^{i\tilde{E}_G\tau}\,\langle\tilde{\Psi}_G|\hat{\mu}_\xi e^{-i\hat{H}\tau}\hat{\mu}_\xi|\tilde{\Psi}_G\rangle$. This line of reasoning shows that only a single SQKFF run will be required for the fast-forwarded prediction of $|\tilde{\psi}(\tau)\rangle = e^{-i\hat{H}\tau}\hat{\mu}_\xi\,|\tilde{\Psi}_G\rangle$.

IV. NUMERICAL EXPERIMENTS

In Fig. 2, we compare the single-reference QKFF and multireference SQKFF algorithms for prototypical quantum chemistry Hamiltonians consisting of a H_2O molecule with fixed bond angle $\phi = 104.45$ [Fig. 2(a)], a BeH_2 molecule [Fig. 2(b)], and a linear hydrogen chain [Fig. 2(c)]. In all three cases, the bond length is chosen to be equal to 1.85 Å. Details of the quantum chemistry Hamiltonian, basis sets, and active space selection for these systems are given in Appendix A of our previous work [31]. It is important to note that due to various symmetries inherent in the quantum chemistry Hamiltonian, the dynamics will be constrained to a symmetry sector that is smaller than the full Hilbert space. The dimension of the symmetry sector will be equivalent to the full configuration interaction (CI) space $\binom{n}{\eta_\alpha}\binom{n}{\eta_\beta}$, where n corresponds to the number of spatial orbitals and η_α (η_β) corresponds to the number of α (β) electrons. For H_2O, BeH_2, and H_6 with active spaces (number of electrons, number of spatial orbitals) of (8,6), (4,6), and (6,6) under a closed-shell configuration, the full CI space will have dimensions $\binom{6}{4}\binom{6}{4} = 225$, $\binom{6}{2}\binom{6}{2} = 225$, and $\binom{6}{3}\binom{6}{3} = 400$, respectively. Here, we focus on the fast-forwarded prediction of the autocorrelation function, $C(t) = \langle\psi(0)|\psi(t)\rangle$, using numerical state vector simulations with ideal time-evolution circuits. Future work will provide a more detailed analysis of the Trotter error, shot-noise error, and other hardware noise effects. For Figs. 2(a) and 2(b), the fast-forwarded prediction used the Krylov subspace dimension, $M = 6$, while Fig. 2(c) used the maximum Krylov dimension, $M = 10$. For all simulations, the single-determinant Hartree-Fock state was used as the initial state unless otherwise specified. In general, we found similar behavior for different single-determinant and bit-string initial states as well as more complicated initial states such as the dipole moment ground-state wave function used in Fig. 5 below. A more general analysis of the fast-forwarding prediction capabilities of the SQKFF algorithm based on the initial state is left for future work.

Reference states were added with the selection process discussed above. The top four rows display the explicit time-evolved correlation function with a different number of reference states. The bottom row displays the infidelity of the true wave function with respect to the QKFF wave function, where the state fidelity is defined as $F(t) = |\langle\psi(t)|\psi_K(t)\rangle|^2$. From the top row of Fig. 2, it is clear that the single-reference fast-forwarded prediction (red line) matches the true correlation function (black line) for only extremely short times. As additional reference states are added, we observe that the predicted autocorrelation function more closely aligns with the true correlation function. We emphasize that this increased fidelity does not require additional circuit depth and requires only additional calls to the quantum computer to estimate the projected subspace matrix elements $[\mathbf{H}]_{n'r',nr}$ and $[\mathbf{S}]_{n'r',nr}$.

Before continuing, it is useful to understand the percentage of full CI space required to generate these long-time predictions. In all cases, we define this percentage as $RM/\binom{n}{\eta_\alpha}\binom{n}{\eta_\beta}$ (recall that R is the number of reference states and M is the Krylov subspace dimension). For H_2O, we get percentages of 2.7%, 16%, 29.3%, and 42.7% for the four cases considered in Fig. 2(a). For BeH_2, the percentages correspond

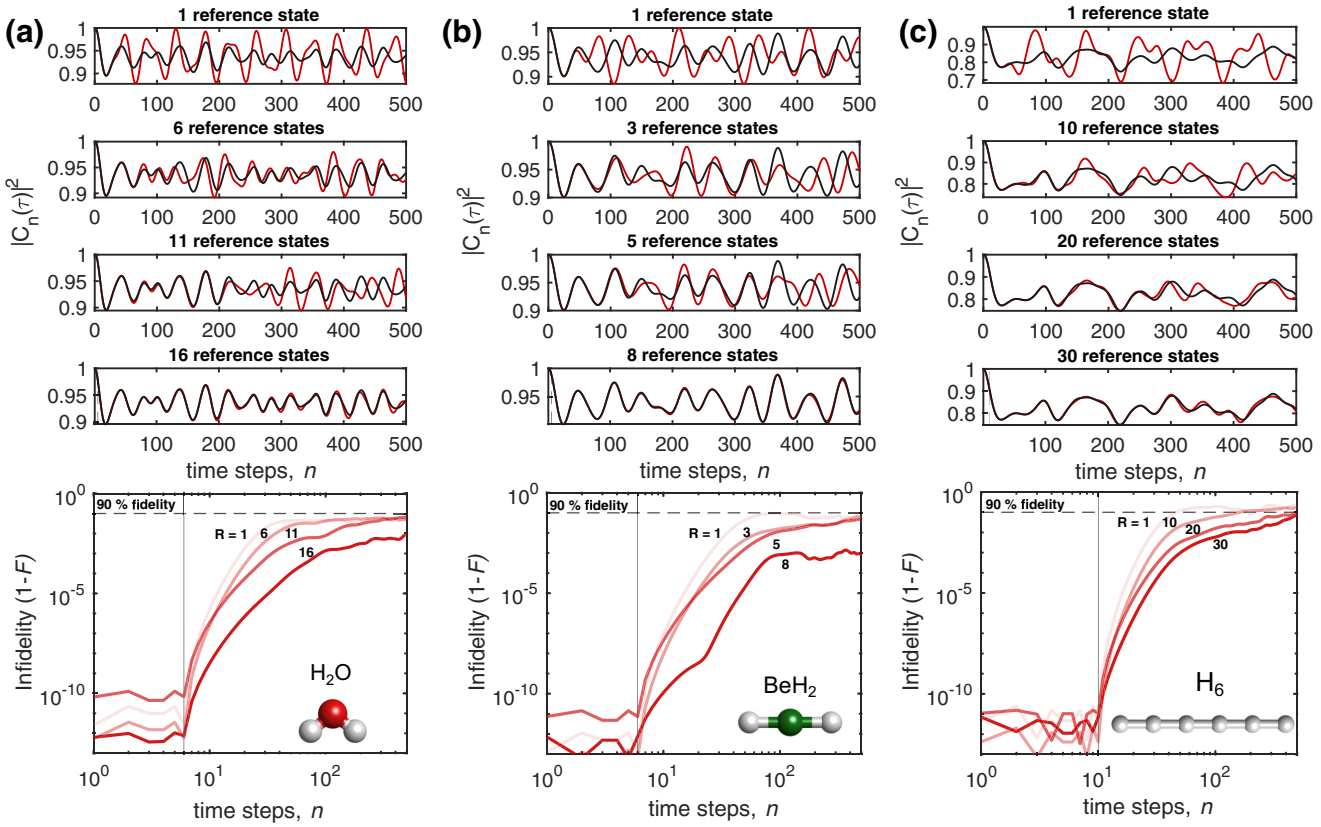

FIG. 2. Fast-forwarding of the autocorrelation function, $C_n(\tau) = \langle\psi(0)|\psi(n\tau)\rangle$, for (a) the H_2O molecule, (b) the BeH_2 molecule, and (c) the H_6 hydrogen chain. The top four rows denote the absolute value squared of the autocorrelation function for various numbers of reference states. The bottom row displays the infidelity of the true wave function $|\psi(t)\rangle$ with respect to the SQKFF predicted wave function, $|\psi_K(t)\rangle$. In all cases, a time step size of $\tau = 0.1$ a.u. was used. For (a) and (b), the fast-forwarded prediction used the Krylov subspace dimension, $M = 6$, while (c) used the maximum Krylov dimension, $M = 10$. In all cases, the single-determinant Hartree-Fock state was used as the initial state.

to 2.7%, 8%, 13.3%, and 21.2% for the four cases considered in Fig. 2(b). For H_6, the percentages correspond to 2.5%, 25%, 50%, and 75%. In all cases, these percentages serve to illustrate the point that while our method works as intended, the convergence tends to be quite slow with regard to the number of reference states required. Future work will explore alternative approaches for reference-state selection that may improve upon this convergence, although it is important to note that, in general, fast-forwarding will be constrained by certain no-go theorems [45,46] and our method merely serves to extract the most information from a small number of time steps n required for a maximum prediction time $T_{\max}$.

In this regard, the route towards high-fidelity, long-time quantum simulation can be achieved in two distinct ways: (1) increasing the Krylov subspace dimension M or (2) increasing the number of reference states R. Ultimately, this leads to a trade-off between quantum and classical complexity for obtaining reliable high-fidelity, long-time predictions. In Fig. 3, we highlight this trade-off by calculating the state fidelity for the water molecule as a function of the Krylov dimension M on the y axis and the number of reference states R on the x axis. In all cases, we chose the singular-value threshold $\epsilon = 1 \times 10^{-9}$. In general, however, the singular-value threshold should be optimized for different numbers of reference states and Krylov subspace dimensions since it affects the fidelity prediction. These plots merely serve to provide a proof of concept of the quantum-classical complexity trade-off. In Fig. 3, it is shown that high fidelities above 90% can be achieved by increasing either of the two independent axes. In the near term, in which quantum hardware provides a severe limit on the gate depth, this plot illustrates how

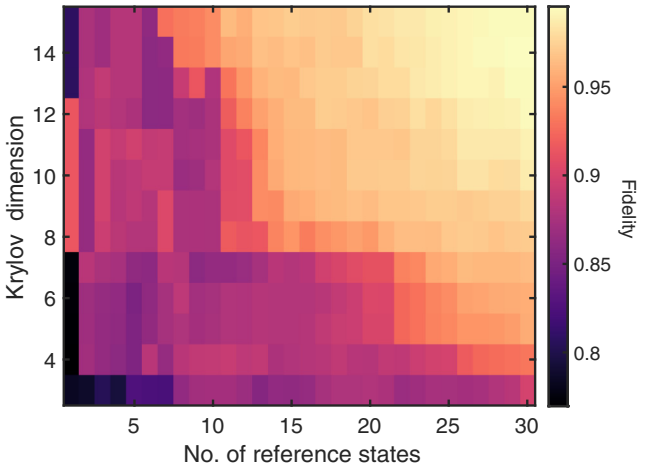

FIG. 3. Trade-off between quantum and classical complexity. Quantum complexity corresponds to circuit depth. Classical complexity is proportional to the number of reference states.

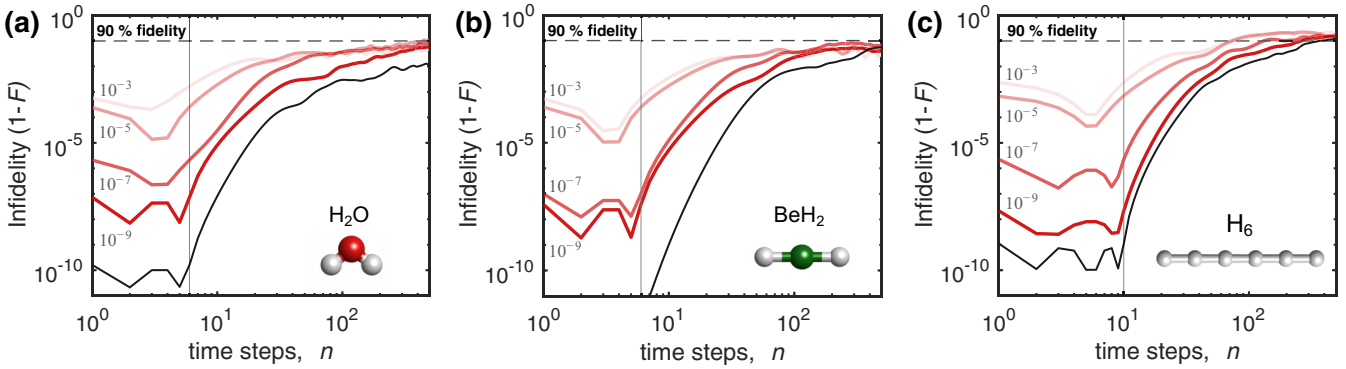

FIG. 4. Noise robustness of the SQKFF algorithm for the same molecular systems as in Fig. 2. For each of the molecular systems, the calculations were performed using a total of (a) 16, (b) 8, and (c) 30 reference states with time step size $\tau = 0.1$ a.u. Additive complex Gaussian noise with zero mean and standard deviation $\sigma = \{10^{-3}, 10^{-5}, 10^{-7}, 10^{-9}\}$ is included for all of the matrix elements of **H** and **S**. A singular-value threshold of (a) $\epsilon = \{1.5, 1.5 \times 10^{-2}, 1.5 \times 10^{-4}, 1.5 \times 10^{-6}, 1.5 \times 10^{-8}\}$, (b) $\epsilon = \{10^{0}, 10^{-2}, 10^{-4}, 10^{-6}, 10^{-8}\}$, and (c) $\epsilon = \{10^{-1}, 10^{-3}, 10^{-5}, 10^{-7}, 10^{-9}\}$ was used for each of the noise standard deviation parameters.

additional resources can be allocated to a classical computer in order to improve quantum dynamical simulation with higher accuracy.

In addition to the quantum-classical trade-off shown in the previous plot, we also studied the noise robustness of the SQKFF algorithm. In Fig. 4, we plot the infidelity of the H_2O, BeH_2, and H_6 molecules with the same parameters as in Fig. 2 (black lines). To study the effect of random noise, we included additive Gaussian noise with zero mean and standard deviation $\sigma = \{10^{-3}, 10^{-5}, 10^{-7}, 10^{-9}\}$, shown in red. The magnitude of the standard deviation ultimately controls the digit precision of the projected subspace matrix elements $[\mathbf{H}]_{n'r',nr}$ and $[\mathbf{S}]_{n'r',nr}$. For all three molecular systems, we found that the fidelity could still remain close to 90% at long times even with Gaussian noise as large as $\sigma = 10^{-3}$, which highlights the noise robustness of the SQKFF algorithm relevant for near-term quantum hardware.

Finally, we test the SQKFF algorithm for the prediction of the two-time dipole moment correlation function, $\langle \hat{\mu}_\xi(t+\tau)\hat{\mu}(t)\rangle = e^{i\tilde{E}_G\tau}\,\langle\tilde{\Psi}_G|\hat{\mu}_\xi e^{-i\hat{H}\tau}\hat{\mu}_\xi|\tilde{\Psi}_G\rangle$, where, as discussed previously, only a single run of the SQKFF algorithm is required. We emphasize that these plots serve as a proof of concept for this algorithm; however, based on the results in Appendix C, we would recommend using a standard quantum Krylov method for ground- and excited-state energy estimation [25–28,30,31] or excited-state variational quantum eigensolver methods [43,47,48] for the purpose of reconstructing the oscillator strength spectrum with current quantum hardware, especially when only low-lying excited-state energies and oscillator strengths are desired. The advantage of this algorithm would correspond to its black-box nature, where zero knowledge is required to estimate the ground- or excited-state energies for the physical system of interest. In Fig. 5(a), we plot the infidelity of the dipole moment propagated wave function, $|\mu(t)\rangle = e^{-i\hat{H}t}\hat{\mu}\,|\Psi_G\rangle$, with respect to the quantum Krylov wave function for the linear H_6 hydrogen chain with the same parameters as in Fig. 2. In Fig. 5(b), we plot the oscillator strength absorption spectrum, which is defined as the Fourier transform of the time-evolved dipole moment correlation function (see Appendix C for details). To ensure that we obtain a stable and well-defined absorption spectrum, we added finite linewidth to the correlation function discussed in Eq. (C1) in Appendix C, which results in an additional $e^{-\gamma t}$ multiplicative factor, where γ corresponds to the finite linewidth. For all of the numerical experiments, we chose a linewidth equal to $\gamma = 1.5 \times 10^{-2}$ atomic units. Here, we observe the same general trends from the autocorrelation function prediction shown in Fig. 2. While the single-reference QKFF algorithm provides an accurate prediction of the first transition peak [see top panel of Fig. 5(b)], it is not able to accurately predict the higher-energy transition peaks, as highlighted by the black line. As more reference states are added, however, we find that the absorption spectrum more closely aligns with the true absorption spectrum with minor deviations at very high energies. Ultimately, this illustrates that the SQKFF algorithm works well for the prediction of a wide variety of time-dependent observables ranging from the autocorrelation function to the two-time correlation function relevant for a wide variety of physical applications.

V. CONCLUDING REMARKS

To conclude, we have shown that real-time quantum Krylov subspace algorithms can be used to fast-forward quantum simulation well beyond the coherence time of current quantum hardware. We developed a theory quantum Krylov fast-forwarding and proposed a selected quantum Krylov fast-forwarding algorithm that is capable of providing an estimate of time-dependent quantum states, which works especially well when the initial state contains a polynomial number of eigenstates [18,46]. We validated the algorithm with numerical experiments focusing on the calculation of the autocorrelation and dipole moment correlation functions for various molecules. While our work provides a way to study a wide range of time-dependent phenomena with near-term quantum hardware, there remains many important avenues of research for improving the SQKFF algorithm. For instance, while we provided evidence of the noise robustness of the SQKFF algorithm, further work should elaborate on the effects of Trotter error, shot noise, and other realistic hardware imperfections. Furthermore, while our results

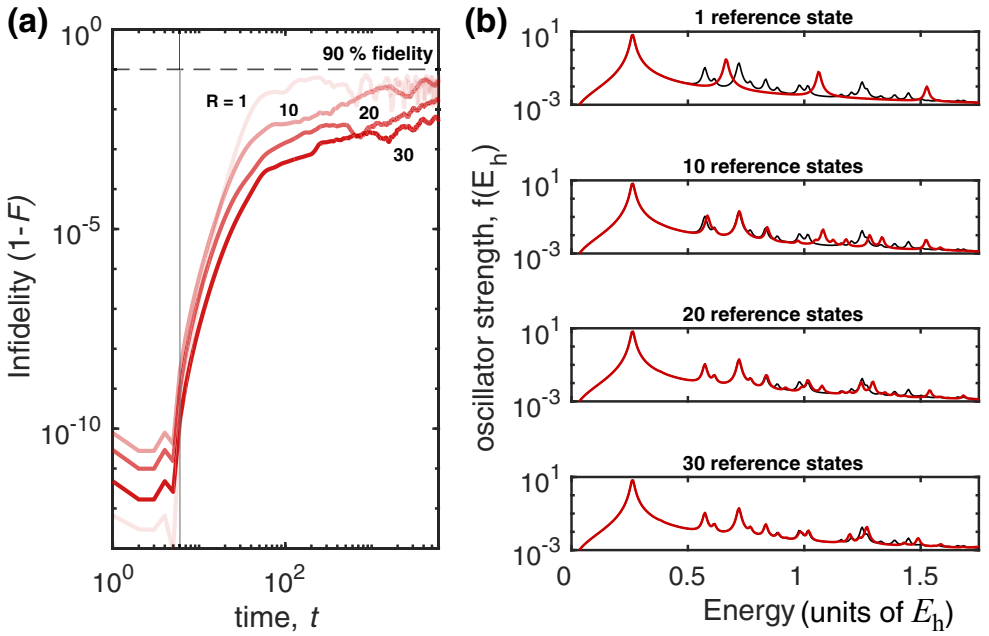

FIG. 5. (a) Infidelity of the dipole moment propagated wave function $|\mu(t)\rangle = e^{-i\hat{H}t}\hat{\mu}\,|\Psi_G\rangle$ compared to the SQKFF prediction for a linear H_6 hydrogen chain. (b) Oscillator strength absorption spectrum with energy in Hartree energy units E_h with different numbers of reference states $R = \{1, 10, 20, 30\}$. In all cases, a Krylov dimension size of $M = 6$ was used along with the time step size $\tau = 0.1$ a.u.

indicate that adding reference states provides a way to achieve long-time, high-fidelity quantum dynamics simulations, the subspace dimension of the proposed algorithms required relatively large subspaces when compared to the symmetry-projected subspaces inherent in the chemical systems. Even for these modest systems, the choice of individual bit strings as reference states resulted in relatively slow convergence, and therefore, alternative approaches may be required for larger systems. Further work should focus on providing a systematic study of the choice of the selection process and reference states in order to improve the SQKFF algorithm's performance. Additional work should also aim to develop and extend this algorithm so that it becomes applicable to time-dependent Hamiltonians.

ACKNOWLEDGMENTS

This material is based upon work supported by Laboratory Directed Research and Development (LDRD) funding from Argonne National Laboratory, provided by the Director, Office of Science, of the U.S. Department of Energy under Contract No. DE-AC02-06CH11357 and the U.S. Department of Energy, Office of Science, Office of Advanced Scientific Computing Research and Office of Basic Energy Sciences, Scientific Discovery through the Advanced Computing (SciDAC) program under Award No. DE-SC0022263. Work performed at the Center for Nanoscale Materials, a U.S. Department of Energy Office of Science User Facility, was supported by the U.S. DOE, Office of Basic Energy Sciences, under Contract No. DE-AC02-06CH11357.

APPENDIX A: SINGULAR-VALUE DECOMPOSITION

For completeness, we outline the approach taken for the construction of the inverse of the complex (Hermitian) overlap matrix $\mathbf{S}$ based on singular-value decomposition (SVD) as suggested in Ref. [30]. The complex SVD of $\mathbf{S}$ is [37,38]

$$\mathbf{S} = \mathbf{U}\mathbf{D}\mathbf{V}^{\dagger}, \tag{A1}$$

where $\mathbf{U}$ and $\mathbf{V}$ are unitary matrices, $\mathbf{D}$ is a diagonal matrix with real elements (called the singular values), $\mathbf{D} = \mathrm{diag}(d_1, d_2, \ldots, d_K)$, and $\dagger$ denotes the Hermitian conjugate (or conjugate transpose). In the present case, the dimension of all matrices is $K \times K$, where $K = MR$, as discussed in the main text. As the matrix $\mathbf{S}$ becomes ill conditioned owing to linear dependencies in the Krylov vectors, one or more of the $\{d_j\}$ can become quite small relative to the largest singular values. If a small positive threshold ϵ is introduced, one can set to zero all the $\{d_j\}$ in $\mathbf{D}$ that are $\leqslant \epsilon$ and still obtain an excellent description of $\mathbf{S}$ via Eq. (A1).

The appropriate inverse of $\mathbf{S}$ is then computed as

$$\mathbf{S}^{-1} = \mathbf{V}\mathbf{D}^{-1}\mathbf{U}^{\dagger}, \tag{A2}$$

where $\mathbf{D}^{-1} = \mathrm{diag}(1/d_1, 1/d_2, \ldots, 1/d_K)$, but such that whenever d_j is zero, the corresponding $1/d_j$ is also set to zero. This well-established approach in numerical analysis, although slightly nonintuitive, effectively represents $\mathbf{S}$ and $\mathbf{S}^{-1}$ in a lower-dimension space that is not ill conditioned. For the majority of the simulations in Sec. IV of the main text, a threshold of $\epsilon = 1 \times 10^{-9}$ was used unless specified otherwise.

APPENDIX B: DIPOLE MOMENT OPERATOR

The dipole moment coefficients μ_{pq} consist of one-electron integrals which can be defined explicitly as $\mu_{pq} = \int d\sigma\ \phi_p^*(\sigma)(-e\mathbf{r})\phi_q(\sigma)$, where σ is a generalized coordinate

consisting of the spatial and spin degrees of freedom, $\sigma = (\mathbf{r}, s)$, while the function $\phi(\sigma)$ represents a one-electron spin orbital. These quantities can be calculated using standard PYTHON packages such as PYSCF [49].

APPENDIX C: RELATION TO THE LINEAR ABSORPTION SPECTRUM

Consider Fermi's golden-rule expression for the line-shape function for incident radiation polarized in the ξth direction ($\xi \in \{x, y, z\}$, $\hbar = 1$):

$$I_\xi(\omega) = \sum_{i,f} \rho_i |\langle \psi_i | \hat{\mu}_\xi | \psi_f \rangle|^2 \delta(E_f - E_i - \omega), \tag{C1}$$

where E_i and E_f correspond to the energies of the initial and final electronic states and ω is the frequency of the incident radiation. Here, ρ_i is the Boltzmann factor for describing a system initially in thermal equilibrium. At zero temperature, the Boltzmann factor is equal to 1 for the ground-state $|\psi_G\rangle$ and 0 everywhere else, reducing the above equation to

$$I_\xi(\omega) = \sum_{f} |\langle \psi_G | \hat{\mu}_\xi | \psi_f \rangle|^2 \delta(E_f - E_G - \omega). \tag{C2}$$

Using $\delta(\omega) = \int_{-\infty}^{\infty} e^{-i\omega t}\, dt$, we make the following simplifications:

$$\begin{aligned} I(\omega) &= \int_{-\infty}^{\infty} e^{-i(E_f - E_G - \omega)t} \sum_f |\langle \psi_G | \hat{\mu}_\xi | \psi_f \rangle|^2 \, dt \\ &= \int_{-\infty}^{\infty} e^{i(E_G+\omega)t} \sum_f \langle \psi_G | \hat{\mu}_\xi e^{-i\hat{H}t} | \psi_f \rangle \langle \psi_f | \mu_\xi | \psi_G \rangle \, dt \\ &= \int_{-\infty}^{\infty} e^{i(E_G+\omega)t} \langle \psi_G | \hat{\mu}_\xi e^{-i\hat{H}t} \mu_\xi | \psi_G \rangle \, dt \\ &= \int_{-\infty}^{\infty} e^{i(E_G+\omega)t} \langle \mu_\xi(0) | \mu_\xi(t) \rangle \, dt, \end{aligned} \tag{C3}$$

where $|\mu_\xi(t)\rangle = e^{-i\hat{H}t} \hat{\mu}_\xi |\psi_G\rangle$. An absorption spectrum or oscillator strength can then be extracted from the real part of the line-shape function,

$$f(\omega) = \frac{2}{3} \omega \sum_\xi \mathrm{Re}[I_\xi(\omega)]. \tag{C4}$$

This result shows how the dipole moment autocorrelation function is related to absorption spectrum. It should be noted that the initial state should ideally correspond to the electronic ground-state wave function.

[1] D. W. Berry, A. M. Childs, R. Cleve, R. Kothari, and R. D. Somma, Simulating Hamiltonian Dynamics with a Truncated Taylor Series, Phys. Rev. Lett. **114**, 090502 (2015).

[2] G. H. Low and I. L. Chuang, Optimal Hamiltonian Simulation by Quantum Signal Processing, Phys. Rev. Lett. **118**, 010501 (2017).

[3] G. H. Low and N. Wiebe, Hamiltonian simulation in the interaction picture, arXiv:1805.00675

[4] D. W. Berry, C. Gidney, M. Motta, J. R. McClean, and R. Babbush, Qubitization of arbitrary basis quantum chemistry leveraging sparsity and low rank factorization, Quantum **3**, 208 (2019).

[5] G. H. Low and I. L. Chuang, Hamiltonian simulation by qubitization, Quantum **3**, 163 (2019).

[6] J. Lee, D. W. Berry, C. Gidney, W. J. Huggins, J. R. McClean, N. Wiebe, and R. Babbush, Even more efficient quantum computations of chemistry through tensor hypercontraction, PRX Quantum **2**, 030305 (2021).

[7] J. Preskill, Quantum computing in the NISQ era and beyond, Quantum **2**, 79 (2018).

[8] B. Bauer, S. Bravyi, M. Motta, and G. K.-L. Chan, Quantum algorithms for quantum chemistry and quantum materials science, Chem. Rev. **120**, 12685 (2020).

[9] M. Cerezo, A. Arrasmith, R. Babbush, S. C. Benjamin, S. Endo, K. Fujii, J. R. McClean, K. Mitarai, X. Yuan, L. Cincio, and P. J. Coles, Variational quantum algorithms, Nat. Rev. Phys. **3**, 625 (2021).

[10] K. Bharti, A. Cervera-Lierta, T. H. Kyaw, T. Haug, S. Alperin-Lea, A. Anand, M. Degroote, H. Heimonen, J. S. Kottmann, T. Menke, W.-K. Mok, S. Sim, L.-C. Kwek, and A. Aspuru-Guzik, Noisy intermediate-scale quantum algorithms, Rev. Mod. Phys. **94**, 015004 (2022).

[11] M. Motta and J. E. Rice, Emerging quantum computing algorithms for quantum chemistry, Wiley Interdiscip. Rev.: Comput. Mol. Sci. **12**, e1580 (2021).

[12] K. Heya, K. M. Nakanishi, K. Mitarai, and K. Fujii, Subspace variational quantum simulator, arXiv:1904.08566.

[13] X. Yuan, S. Endo, Q. Zhao, Y. Li, and S. C. Benjamin, Theory of variational quantum simulation, Quantum **3**, 191 (2019).

[14] S. Endo, J. Sun, Y. Li, S. C. Benjamin, and X. Yuan, Variational Quantum Simulation of General Processes, Phys. Rev. Lett. **125**, 010501 (2020).

[15] M. Otten, C. L. Cortes, and S. K. Gray, Noise-resilient quantum dynamics using symmetry-preserving ansatzes, arXiv:1910.06284.

[16] C. Cîrstoiu, Z. Holmes, J. Iosue, L. Cincio, P. J. Coles, and A. Sornborger, Variational fast forwarding for quantum simulation beyond the coherence time, npj Quantum Inf. **6**, 82 (2020).

[17] B. Commeau, M. Cerezo, Z. Holmes, L. Cincio, P. J. Coles, and A. Sornborger, Variational Hamiltonian diagonalization for dynamical quantum simulation, arXiv:2009.02559.

[18] J. Gibbs, K. Gili, Z. Holmes, B. Commeau, A. Arrasmith, L. Cincio, P. J. Coles, and A. Sornborger, Long-time simulations with high fidelity on quantum hardware, arXiv:2102.04313.

[19] L. Bittel and M. Kliesch, Training Variational Quantum Algorithms Is NP-Hard, Phys. Rev. Lett. **127**, 120502 (2021).

[20] J. R. McClean, S. Boixo, V. N. Smelyanskiy, R. Babbush, and H. Neven, Barren plateaus in quantum neural network training landscapes, Nat. Commun. **9**, 4812 (2018).

[21] S. Wang, E. Fontana, M. Cerezo, K. Sharma, A. Sone, L. Cincio, and P. J. Coles, Noise-induced barren plateaus in variational quantum algorithms, Nat. Commun. **12**, 6961 (2021).

[22] M. Cerezo, A. Sone, T. Volkoff, L. Cincio, and P. J. Coles, Cost function dependent barren plateaus in shallow parametrized quantum circuits, Nat. Commun. **12**, 1791 (2021).

[23] A. Arrasmith, M. Cerezo, P. Czarnik, L. Cincio, and P. J. Coles, Effect of barren plateaus on gradient-free optimization, Quantum **5**, 558 (2020).

[24] J. R. McClean, M. E. Kimchi-Schwartz, J. Carter, and W. A. de Jong, Hybrid quantum-classical hierarchy for mitigation of decoherence and determination of excited states, Phys. Rev. A **95**, 042308 (2017).

[25] W. J. Huggins, J. Lee, U. Baek, B. O'Gorman, and K. B. Whaley, A non-orthogonal variational quantum eigensolver, New J. Phys. **22**, 073009 (2020).

[26] R. M. Parrish and P. L. McMahon, Quantum filter diagonalization: Quantum eigendecomposition without full quantum phase estimation, arXiv:1909.08925.

[27] N. H. Stair, R. Huang, and F. A. Evangelista, A multireference quantum Krylov algorithm for strongly correlated electrons, J. Chem. Theory Comput. **16**, 2236 (2020).

[28] J. Cohn, M. Motta, and R. M. Parrish, Quantum filter diagonalization with double-factorized hamiltonians, PRX Quantum **2**, 040352 (2021).

[29] E. N. Epperly, L. Lin, and Y. Nakatsukasa, A theory of quantum subspace diagonalization, SIAM J. Matrix Anal. Appl. **43**, 1263 (2022).

[30] K. Klymko, C. Mejuto-Zaera, S. J. Cotton, F. Wudarski, M. Urbanek, D. Hait, M. Head-Gordon, K. B. Whaley, J. Moussa, N. Wiebe, W. A. de Jong, and N. M. Tubman, Real-time evolution for ultracompact hamiltonian eigenstates on quantum hardware, PRX Quantum **3**, 020323 (2022).

[31] C. L. Cortes and S. K. Gray, Quantum Krylov subspace algorithms for ground-and excited-state energy estimation, Phys. Rev. A **105**, 022417 (2022).

[32] E. A. Ruiz Guzman and D. Lacroix, Accessing ground-state and excited-state energies in a many-body system after symmetry restoration using quantum computers, Phys. Rev. C **105**, 024324 (2022).

[33] M. Motta, C. Sun, A. T. Tan, M. J. O'Rourke, E. Ye, A. J. Minnich, F. G. Brandão, and G. K.-L. Chan, Determining eigenstates and thermal states on a quantum computer using quantum imaginary time evolution, Nat. Phys. **16**, 205 (2020).

[34] T. J. Park and J. Light, Unitary quantum time evolution by iterative Lanczos reduction, J. Chem. Phys. **85**, 5870 (1986).

[35] K. H. Lim, T. Haug, L. C. Kwek, and K. Bharti, Fast-forwarding with NISQ processors without feedback loop, Quantum Sci. Technol. **7**, 015001 (2022).

[36] J. C. Butcher, *Numerical Methods for Ordinary Differential Equations* (Wiley, Hoboken, NJ, 2016).

[37] L. N. Trefethen and D. Bau, *Numerical Linear Algebra* (Society for Industrial and Applied Mathematics, Philadelphia, PA, 1997).

[38] P. A. Businger and G. H. Golub, Algorithm 358: Singular value decomposition of a complex matrix, Commun. ACM **12**, 564 (1969).

[39] W. Meyer and P. Rosmus, PNO–CI and CEPA studies of electron correlation effects. III. Spectroscopic constants and dipole moment functions for the ground states of the first-row and second-row diatomic hydrides, J. Chem. Phys. **63**, 2356 (1975).

[40] S. T. Hess, S. Huang, A. A. Heikal, and W. W. Webb, Biological and chemical applications of fluorescence correlation spectroscopy: A review, Biochemistry **41**, 697 (2002).

[41] I. Kassal, J. D. Whitfield, A. Perdomo-Ortiz, M.-H. Yung, and A. Aspuru-Guzik, Simulating chemistry using quantum computers, Annu. Rev. Phys. Chem. **62**, 185 (2011).

[42] G. Rickayzen, *Green's Functions and Condensed Matter* (Dover Publications, Mineola, New York, 2013).

[43] R. M. Parrish, E. G. Hohenstein, P. L. McMahon, and T. J. Martínez, Quantum Computation of Electronic Transitions Using a Variational Quantum Eigensolver, Phys. Rev. Lett. **122**, 230401 (2019).

[44] F. Jamet, A. Agarwal, and I. Rungger, Quantum subspace expansion algorithm for Green's functions, arXiv:2205.00094.

[45] Y. Atia and D. Aharonov, Fast-forwarding of Hamiltonians and exponentially precise measurements, Nat. Commun. **8**, 1572 (2017).

[46] S. Gu, R. D. Somma, and B. Şahinoğlu, Fast-forwarding quantum evolution, Quantum **5**, 577 (2021).

[47] K. M. Nakanishi, K. Mitarai, and K. Fujii, Subspace-search variational quantum eigensolver for excited states, Phys. Rev. Res. **1**, 033062 (2019).

[48] O. Higgott, D. Wang, and S. Brierley, Variational quantum computation of excited states, Quantum **3**, 156 (2019).

[49] Q. Sun *et al.*, Recent developments in the PySCF program package, J. Chem. Phys. **153**, 024109 (2020).